On the precision of neural computation with interaural time differences in the medial superior olive

Petr Marsalek[a,b,e], (Marek Hajny)[a,e], Zbynek Bures[c,d]

[a] *Institute of Pathological Physiology, First Medical Faculty, Charles University in Prague, U Nemocnice 5/478, 128 53, Praha 2, Czech Republic*
[b] *Department of Radioelectronics, Faculty of Electrical Engineering, Czech Technical University in Prague, Technická 2/1902, 16627, Praha 6, Czech Republic*
[c] *Czech Institute of Informatics, Robotics and Cybernetics, Czech Technical University in Prague, Jugoslávských partyzánů 4/1903, 166 36, Praha 6, Czech Republic*
[d] *College of Polytechnics, Tolstého 16/1556, 586 01, Jihlava, Czech Republic*
[e] *Corresponding authors: Petr.Marsalek@LF1.CUni.CZ, Marek.Hajny@LF1.CUni.CZ*

Abstract

We study a model of mammalian sound source localization in horizontal plane. Experiments on small rodents indicate that mammals use broadly tuned channels of azimuth for localization in horizontal plane. In mammals this neural computation is implemented by medial superior olive for low frequency sounds up to 1500 Hz. It has been shown previously that spike timing jitter, coincidence detection window length, sound frequency, among other input parameters, influence the output precision, measured by the just noticeable difference in output of the circuit. We use stochastic model with spiking neurons. We explore variations of the parameters mentioned above. We calculate properties of the model with the use of analytical methods. Predictions of this model have straightforward applications in testing and designing stimulation protocols used in cochlear implants.

Keywords: binaural hearing, coincidence detection, ergodic hypothesis, ideal observer, interaural time difference, just noticeable difference, medial superior olive, neuronal arithmetic, sound localization

1. Introduction

Mammalian sound localization circuits contain two nuclei in the auditory brainstem, the medial and the lateral superior olive (MSO and LSO). Neurons in these nuclei are the first binaural neurons in the auditory pathway, they are connected to both ears.

This article presents description of information encoding and neural computation in the MSO obtained mostly with analytical computations. Using the

analytical tools we extend quantitative results obtained by Sanda and Marsalek (2012) only in simulations and connect them to Bures and Marsalek (2013) to arrive to unified description of neural circuits in the superior olive. We use this description to find maximum spike timing precision attained by the following two respective modalities (low and high frequency sound localization) of natural and electrical hearing.

Due to the physical nature of the binaural sound, the MSO neurons process spike timing differences in the range of tens of microseconds, μs. The MSO processes low frequency sounds, in human this is from 20 Hz to not more than 2 kHz. The LSO processes high frequency sounds, in human this is from 1 kHz up to 20 kHz. The overlapping region is known to have a sensitivity drop at 1.5 kHz Mills (1958).

Firing rate, first spike latency and individual spike timings are used in neural system coding, especially in the auditory pathway. The highest known spike timing precision that has been proven to be utilized in the mammalian auditory system is the motor response in a bat. In behavioral experiment, the big brown bat, *Eptesicus fuscus* catches tidbit larvae of the meal-worm beetle *Tenebrio molitor*. The motor precision is in the range of hundreds of nanoseconds, ns, and auditory separation of ultrasound echoes is in the order of microsecond units, 1 μs Simmons et al. (1998). Comparable performance of the human MSO is in the range of microseconds, 10 μs and can be improved after several hours of training.

Different neural mechanisms are employed in the two nuclei.

It has been reported that computation in the MSO is independent on sound intensity Grothe et al. (2010). With higher sound intensity, first spike latency is shortening. Relation of this dependence to ITD and ILD has been described, yet it is difficult to interpret. Michelet et al. (2012) have shown the latencies in experiment on the domestic cat, *Felis silvestris*.

The LSO and MSO extract location information with the use of different physical cues. The sensitivity of the system in dependence on the main sound frequency to sounds of different main frequencies should be different. In human, MSO is the larger of the two nuclei and contains approximately 15500 neurons, human LSO contains 5600 neurons.

We have previously studied parameter free models of human sound localization. Current development of binaural cochlear implant technology enables to stimulate auditory periphery with rich repertoire of patterns. Better understand-

ing to the MSO mechanisms will help to improve electrical hearing.

Moving sound objects are localized using the ITD and ILD cues and in addition to this, Doppler effect pitch changes signal approaching and retreating objects, even though Doppler cues are less salient. Due to these phenomena, neural circuits are robust to pitch variation. It is therefore interesting to pose a question, whether wider pitch changes in a thought experiment in rescaling time will affect these neural mechanisms. Speeding up, or slowing down the system time can be extended to two octaves up and down the regular time, see Table 2.

The range of sound frequencies processed in the MSO circuit is limited to the low frequency band. In human, where audible sound frequencies range from 20 Hz to 20 kHz, this low frequency band spans from 20 Hz to 1.5 kHz. Moreover, in the marginal values of this interval, performance of sound azimuth discrimination is worse. It is generally agreed that the main reason, why the workings of the MSO circuit deteriorate towards higher frequency is lowering of the synchronization of spike trains in the circuit with the sound source phase. The synchronization between two corresponding series of point events can be expressed as a (discrete version of) vector strength, defined below in equation (5).

2. Results

We investigate how circuit output and overall performance depend on sound frequency and sound intensity. Figure 1 shows an example of typical vector strength lowering towards higher frequencies, as observed in the auditory nerve (AN). The prevailing majority of neurons in the auditory pathway has a vector strength spike train statistics sigmoidally dropping towards higher sound frequencies as it is in this example. In this figure, data recorded by Joris (1996) from the MSO in cat were fitted to the sigmoidal curve with the general formula of the Boltzmann function used in Marsalek and Lansky (2005). The curve fit of vector strength r_{V} in dependence on sound frequency f_{S} is:

$$r_{\mathrm{V}} = (1 + \exp(K_{\mathrm{S}} f_{\mathrm{S}} - K_{\mathrm{C}} F_{\mathrm{C}}))^{-1}, \tag{1}$$

where K_{S} (sound coefficient) and K_{C} (critical coefficient), F_{C} (critical half frequency) are proportionality constants.

Figure 2 shows the best just noticeable difference (JND) obtained with the basic parameter set in dependence on the sound frequency. The quadratic curve fit of the JND denoted Δt_{JND} is:

$$\Delta t_{\mathrm{JND}} = A(f_{\mathrm{S}} - F_{\mathrm{C}})^2 + B, \tag{2}$$

where A and B are fitted constants and the other parameters and variables are as above. See also Zwislocki and Feldman (1956).

Figure 3 shows how ITD JND depends on timing jitter τ_{J}. There is one critical $\tau_{\mathrm{J}} = 0.2$ and one optimal value (normalized to $\tau_{\mathrm{J}} = 1$) of timing jitter related to the output JND and firing rate. Simulations show that with lowering timing jitter the circuit output is virtually more and more precise. The two curves fitted to the simulation are:

1. fit of exponential function to simulations:

$$\Delta t_{\mathrm{JND}} = \exp(A_1(\tau_{\mathrm{J}} - B_1)) - C_1, \tag{3}$$

where $A_1 = 1.9$, $B_1 = 1.25$ and $C_1 = 0.2$ are fitted parameters. This is shown conveniently by the logarithmic y-axis in this figure.

2. Another fit, which also takes into account shot noise in lower jitter values, is to a quadratic function:

$$\Delta t_{\mathrm{JND}} = A_2(\tau_{\mathrm{J}} - B_2)^2 + C_2, \tag{4}$$

where $A_2 = 2.5$, $B_2 = 1$, $C_2 = 1$. There is only one parameter (A) fitted to data, as the point $(x, y) = (B_2, C_2)$ has been chosen to be a unit, this fit is a normalized fit of the model.

Logarithm of the simulated JND lowers with the exponential curve (3), which is concave function of jitter τ_{J} as the jitter gets lower. The trend towards higher accuracy diverges from the parabolic fit (4), when jitter reaches critical value between $0.2 \lessapprox \tau_{\mathrm{J}} \lessapprox 0.5$ ms. Beyond that point towards the lower jitter values, the neural circuit cannot function properly, as too low jitter prevents the interaction of spikes from the left and right side within the coincidence detection mechanism.

Figure 4 shows the calibration curve. The rising slope of this curve is used as a readout function yielding th firing rate in dependency on the ITD which in turn signals the sound azimuth to the next nuclei up to the auditory pathway.

Comment

TO-DO - This Table X should be extended: more parameters and range of parameters...

Table number One-and-one-half:

Top description (x-axis)

a 1) normal hearing

b 2) hearing impaired

c 3) electrical - no jitter

d 4) artificial jitter
e 5) (sub)optimal jitter
Side description (y-axis)
1) 40 - 160 Hz
2) 160 - 640 Hz
3) 640 - 2,560 Hz
4) 2,560 - 10,240 Hz

3. Discussion

3.1. Things to do

First: Reproduce the curve in panel with sound frequency on x-axis and JND on the y-axis in Fig. 2.

Second: Present the curve from the right panel of Fig.4 from Sanda P., Jitter Effect on the Performance..., as part of Fig. 3.

Some other tentative questions: What is the highest slope of the ITD interpolation curve, such that it gives the resolution of 4° (angular degrees)?

(This we will do later: We also discuss the relation of the MSO neural circuit to its neighboring nucleus, the LSO, and its output.)

Cite: Mlynarski and Jost (2014)...

4. Experimental Procedures

4.1. Preliminaries

Our procedures are mostly in using computational models, experimental data and statistical methods. Here we list several assumptions used in the paper.

(1) Single MSO neuron constants, see Toth and Marsalek (2015). (2) Synaptic machinery, see Toth and Marsalek (2015). (3) Ergodic assumption see Sanda and Marsalek (2012).

4.2. Vector strength

The vector strength is defined as it is used since Goldberg and Brown (1969). Let us have sample (spike) phases φ_i, $i = 1, 2, \ldots, N$ relative to phases of a given input master periodic function, which does not enter the formula. (Such function can be for example sound stimulus eliciting the spike train as a response.) (Discrete sum) vector strength of sample $\varphi_1, \ldots, \varphi_N$ is defined as

$$r_{\mathrm{V}}(\varphi_i) = \frac{1}{N}\sqrt{\left(\sum_{i=1}^{N}\cos\varphi_i\right)^2 + \left(\sum_{i=1}^{N}\sin\varphi_i\right)^2}. \tag{5}$$

4.3. Just noticeable differences of ITD

This subsection of Methods should be analogous to the corresponding section in Bures and Marsalek (2013)...

4.4. Model of the MSO neural circuit

To do: Describe model and calculations.

Notes

To Do: Add citations to discussion:

Cite Franken et al. (2014), this is an experimental description of MSO workings in line with our concepts and coincidence detection theories.

Cite Silver (2010), because this is a prospect of neuronal arithmetic.

To do: check, whether both Smith et al. (1991) and Smith et al. (1993) are relevant.

The ergodic paper of Toth et al. (2018) goes to Discussion.

Another MSO model, already in 2005 is: Zhou et al. (2005).

Cochlear implants and MSO: Kerber and Seeber (2012).

Check Wu and Kelly (1992): WHY DO WE CITE THIS?

Here are the three LSO experimental papers, which have detailed methodology applicable to overlap of sound frequency ranges with the MSO Joris and Yin (1995); Joris (1996); Joris and Yin (1998).

Jeffress et al. (1962) goes instead of Jeffress, 1948.

(No)Cite: Bures (2012) is neuronal arithmetic in Biol. Cybern.

(No)Cite: Bures and Marsalek (2013) is "dual" paper in Brain Res.

Do we still need to cite this review: Grothe et al. (2010)?...

Thee are the classics...: Goldberg and Brown (1969).

Cochlear delays, very important: Joris et al. (2006).

Yet another neuronal arithmetic: Koutsou et al. (2012).

This is about other dimension; if we cite this, then we must discuss all the three, Kopco et al. (2012). hall we do that?

Jitter and variability... : Kostal and Marsalek (2010).

This is a chronological record of the neuronal arithmetic ideas, starting from: Marsalek (2000), through Marsalek (2001) some more detailed account o the diversity of cell functions and shapes: Reed et al. (2002), through Marsalek and Kofranek (2004) to the Marsalek and Kofranek (2005); watch the years ...

Remains to be cited: no-cites of Smith et al. (1993).

Next Cariani (2011), Bouse et al. (2019), Bures (2014), Michelet et al. (2012), Srinivasan et al. (2018).

Conclusions

This theoretical paper is a followup of sound localization precision descriptions in the MSO Sanda and Marsalek (2012) and in the LSO Bures and Marsalek (2013). Novel results are two: 1) analytical estimates of results obtained previously only by numerical simulation and 2) comparison of natural and electrical hearing modalities and demonstrating what is the maximum timing precision which can be attained by the two modalities.

Acknowledgments

LaTeX compilation date is: March 21, 2019.
PM and MH were supported by: Charles University graduate students research program (acronym SVV) No. 260371/ 2017-2019. Special thanks to Pavel Sanda for permission to use his simulations.

References

Bouse, J., Vencovský, V., Rund, F., Marsalek, P., 2019. Functional rate-code models of the auditory brainstem for predicting lateralization and discrimination data of human binaural perception. J. Acoust. Soc. Am. 145 (1), 1–15.

Bures, Z., 2012. The stochastic properties of input spike trains control neuronal arithmetic. Biol. Cybern. 106 (2), 111–122.

Bures, Z., 2014. Internal representation and processing of acoustic stimuli in the nervous system. VUTIUM, Brno, Czech Republic, pp. 1–22, Habilitation thesis, ISSN 1213-418X.

Bures, Z., Marsalek, P., 2013. On the precision of neural computation with the interaural level difference in the lateral superior olive. Brain Res. 1536, 111–122.

Bures, Z., Marsalek, P., 2019. Discrimination of sound intensity at low frequencies: models and psychophysics. Biosystems, *submitted,* pages 1-15.

Cariani, P., 2011. Jeffress model. Scholarpedia 6 (7), 2920.

Franken, T. P., Bremen, P., Joris, P. X., 2014. Coincidence detection in the medial superior olive: mechanistic implications of an analysis of input spiking patterns. Front. Neural Circuits 8 (42), 1–21.

Goldberg, J. M., Brown, P. B., 1969. Response of binaural neurons of dog superior olivary complex to dichotic tonal stimuli: some physiological mechanisms of sound localization. J. Neurophysiol. 32 (4), 613–636.

Grothe, B., Pecka, M., McAlpine, D., 2010. Mechanisms of sound localization in mammals. Physiol. Rev. 90 (3), 983–1012.

Jeffress, L. A., Blodgett, H. C., Deatherage, B. H., 1962. Effect of interaural correlation on the precision of centering a noise. J. Acoust. Soc. Am. 34 (8), 1122–1123.

Joris, P. X., Van de Sande, B., Louage, D. H., van der Heijden, M., 2006. Binaural and cochlear disparities. Proc. Natl. Acad. Sci. USA 103 (34), 12917–12922.

Joris, P. X., Yin, T. C., 1995. Envelope coding in the lateral superior olive. I. Sensitivity to interaural time differences. J. Neurophysiol. 73 (3), 1043–1062.

Joris, P. X., 1996. Envelope coding in the lateral superior olive. II. Characteristic delays and comparison with the responses in the medial superior olive. J. Neurophysiol. 76 (4), 2137–2156.

Joris, P. X., Yin, T. C., 1998. Envelope coding in the lateral superior olive. III. Comparison with afferent pathways. J. Neurophysiol. 79 (1), 253–69.

Kerber, S., Seeber, B. U., 2012. Sound localization in noise by normal-hearing listeners and cochlear implant users. Ear Hear. 33 (4), 445–457.

Kopco, N., Huang, S., Belliveau, J. W., Raij, T., Tengshe, C., Ahveninen, J., 2012. Neuronal representations of distance in human auditory cortex. Proc. Natl. Acad. Sci. USA 109 (27), 11019–11024.

Kostal, L., Marsalek, P., 2010. Neuronal jitter: can we measure the spike timing dispersion differently? Chinese J. Physiol. 53 (6), 454–464.

Koutsou, A., Christodoulou, C., Bugmann, G., Kanev, J., 2012. Distinguishing the causes of firing with the membrane potential slope. Neural Comput. 24 (9), 2318–2345.

Krips, R., Furst, M., 2009. Stochastic properties of auditory brainstem coincidence detectors in binaural perception. J. Acoust. Soc. Am. 125 (3), 1567–1583.

Laback, B., Majdak, P., 2008. Binaural jitter improves interaural time-difference sensitivity of cochlear implantees at high pulse rates. Proc. Natl. Acad. Sci. USA 105 (2), 814–817.

Marsalek, P., 2000. Coincidence detection in the Hodgkin-Huxley equations. Biosystems 58 (1-3), 83–91.

Marsalek, P., 2001. Neural code for sound localization at low frequencies. Neurocomputing 38-40 (1-4), 1443–1452.

Marsalek, P., Kofranek, J., 2004. Sound localization at high frequencies and across the frequency range. Neurocomputing 58-60, 999–1006.

Marsalek, P., Kofranek, J., 2005. Spike encoding mechanisms in the sound localization pathway. Biosystems 79 (1-3), 191–8.

Marsalek, P., Lansky, P., 2005. Proposed mechanisms for coincidence detection in the auditory brainstem. Biol. Cybern. 92 (6), 445–451.

Michelet, P., Kovacic, D., Joris, P. X., 2012. Ongoing temporal coding of a stochastic stimulus as a function of intensity: time-intensity trading. J. Neurosci. 32 (28), 9517–9527.

Mills, A. W., 1958. On the minimum audible angle. J. Acoust. Soc. Am. 30 (4), 237–246.

Mlynarski, W., Jost, J., 2014. Statistics of natural binaural sounds. PLoS One 9 (10), e108968, 1–15, ArXiv preprint: 1402.4648.

Reed, M. C., Blum, J. J., Mitchell, C. C., 2002. Precision of neural timing: effects of convergence and time-windowing. J. Comput. Neurosci. 13 (1), 35–47.

Sanda, P., Marsalek, P., 2012. Stochastic interpolation model of the medial superior olive neural circuit. Brain Res. 1434, 257–265.

Silver, R. A., 2010. Neuronal arithmetic. Nat. Rev. Neurosci. 11 (7), 474–489.

Simmons, J. A., Ferragamo, M. J., Moss, C. F., 1998. Echo-delay resolution in sonar images of the big brown bat, *Eptesicus fuscus*. Proc. Natl. Acad. Sci. USA 95 (21), 12647–12652.

Smith, P. H., Joris, P. X., Carney, L. H., Yin, T. C., 1991. Projections of physiologically characterized globular bushy cell axons from the cochlear nucleus of the cat. J. Comp. Neurol. 304 (3), 387–407.

Smith, P. H., Joris, P. X., Yin, T. C. T., 1993. Projections of physiologically characterized spherical bushy cell axons from the cochlear nucleus of the cat: evidence for delay lines to the medial superior olive. J. Comp. Neurol. 331 (2), 245–260.

Srinivasan, S., Laback, B., Majdak, P., Delgutte, B., 2018. Introducing short interpulse intervals in high-rate pulse trains enhances binaural timing sensitivity in electric hearing. J. Assoc. Res. Otolaryngol. 19 (3), 301–315.

Toth, P. G., Marsalek, P., 2015. Analytical description of coincidence detection synaptic mechanisms in the auditory pathway. Biosystems 136, 90–98.

Toth, P. G., Marsalek, P., Pokora, O., 2018. Ergodicity and parameter estimates in auditory neural circuits. Biol. Cybern. 112 (1-2), 41–55.

Wu, S. H., Kelly, J. B., 1992. Synaptic pharmacology of the superior olivary complex studied in mouse brain slice. J. Neurosci. 12 (8), 3084–3097.

Zhou, Y., Carney, L. H., Colburn, H. S., 2005. A model for interaural time difference sensitivity in the medial superior olive: interaction of excitatory and inhibitory synaptic inputs, channel dynamics, and cellular morphology. J. Neurosci. 25 (12), 3046–3058.

Zwislocki, J., Feldman, R., 1956. Just noticeable differences in dichotic phase. J. Acoust. Soc. Am. 28 (5), 860–864, **Circa 34 + 5 = 39 is total references count.**

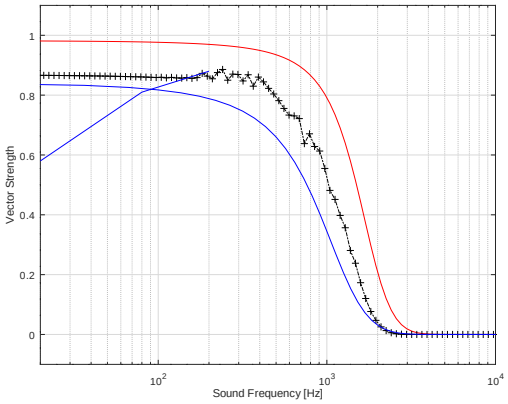

Figure 1: **Vector strength of auditory nerve spike trains in dependence on sound frequency.** X-axis shows fundamental sound frequency in Hz in a logarithmic scale and y-axis shows the vector strength. Even though is some nuclei up the auditory pathway the synchronization can be maintained towards higher frequencies than shown here, the decrease of the vector strength towards higher frequencies is a general property of all neurons in the auditory pathway.

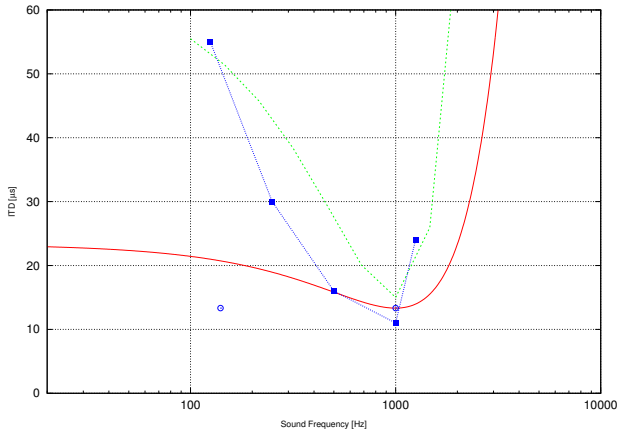

Figure 2: **The shortest ITD detected in the dependence on sound frequency.** X-axis shows sound frequency in Hz in a logarithmic scale and y-axis the shortest JND in μs. This is a theoretical prediction based on the analytical model and basic parameter set used in previous simulations.

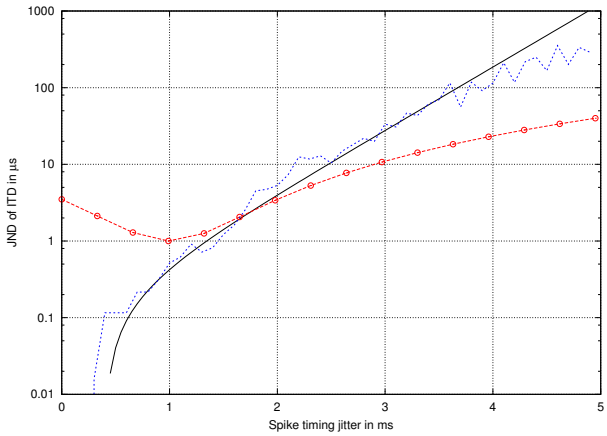

Figure 3: **The JND values in basic parameter set in dependence on the jitter magnitude.** This plot in semi-logarithmic y-scale shows just noticeable difference of interaural time difference depending on variation of the spike timing jitter. Jagged line: simulated data, solid line: an exponential fit to the simulations under the assumption of arbitrary time precision in the model circuit, line with circles: a quadratic function estimate of spike timing precision in a system with addition of noise.

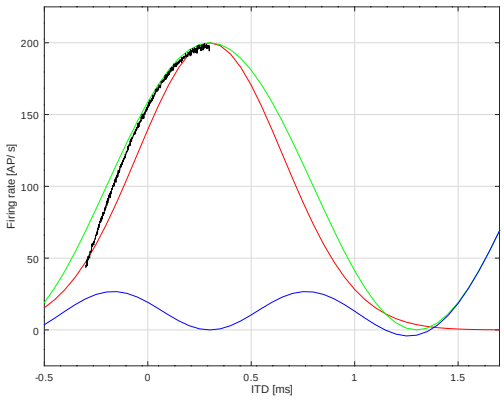

Figure 4: **Gaussian fit of the ITD to firing rate slope calibration curve.** X-axis shows ITD in ms and y-axis shows corresponding firing rate in action potentials per second. Note that the curve peak is offset from the origin of coordinates at $t_{\mathrm{ITD}} = 0$.

Parameter	Symbol	Units	Typical Value	Ranges
Jitter	$T_J = \sigma$	ms	1	0.125 - 8
Window	w_{CD}	ms	0.6	0.15 - 1.5
Sound Frequency	f	Hz	200	40-1600

Table 1: The basic set of parameters.

Parameter	Symbol	Units	4× Slower	Values (man)	4× Faster	16× Faster
Sound frequency ranges	f	Hz	17.5 - 110	70 - 440	280 - 1760	1120 - 7040 Hz
Window size	w_{CD}	μs	2400	600	150	37.5
Timing Jitter	T_{J}	ms	4	1	0.25	62.5 μs
Predicted JND	T	μs	40	10	2.5	N/ A
Predicted detection time*	T	ms	2,600	650	162.5	N/ A

Table 2: TODO add the last OVERLAPPING band 4480 - 28160 and make all a bit narrower to start at 20 Hz and end at 20000 Hz. This Table is direct scaling of parameters used in Sanda and Marsalek (2012). Make also MSO and LSO entries...
Predicted values are: 1) just noticeable difference (JND) of the ITD 2) the time of observation by an ideal observer reading the information from one neuron.